Research Article

Journal of PeptideScience

Received: 20 June 2008 Revised: 23 September 2008 Accepted: 24 September 2008 Published online in Wiley Interscience: 1 December 2008

(www.interscience.com) DOI 10.1002/psc.1084

Molecular dynamics studies of the P pilus rod subunit PapA‡

Luigi Vitagliano,[a] Alessia Ruggiero,[a] Carlo Pedone[a,b] and Rita Berisio[a]*

Adhesion of uropathogenic *Escherichia coli* to host tissues is mediated by pili, which extend from the outer cell membrane of the bacterium. Here we report molecular dynamics (MD) characterizations of the major constituent of P pili from the uropathogenic *E. coli*, PapA, in unliganded state and in complex with the G1 strand of the chaperone PapD. To mimic the PapA response to the gradual dissociation of the PapD G1 strand and to evaluate the role of PapA chaperone recognition sites, we also carried out MD simulations of complexes of PapA with fragments of PapD G1 strand, that leave either the P4 or both P3 and P4 sites unoccupied. Data on the unbound form of PapA indicate that, upon release of the chaperone, PapA evolves toward compact states that are likely not prone to subunit–subunit association. In line with recent experimental reports, this finding implies that chaperone release and subunit–subunit association must be concerted. Our data also indicated that the gradual unbinding of the chaperone from the PapA groove has increasingly strong structural consequences. Indeed, the release of the chaperone from the site P4, which is closest to the initiation site (P5), does not have dramatic effects on the domain structure, whereas its release from both the P4 and the adjacent P3 sites induces a quick structural transition toward a collapsed state, where the subunit groove is obstructed.

Supporting information may be found in the online version of this article

Keywords: protein–protein interactions; donor-strand exchange; chaperone; molecular dynamics; adhesive proteins

Introduction

Uropathogenic strains of *Escherichia coli* are responsible for infections of the bladder (cystitis) and kidney (pyelonephritis), which are among the most common bacterial infections [1]. The survival and persistence of these bacteria in the urinary tract require their efficient attachment to the host cells. To this scope, bacteria have developed a variety of different adhesive extensions. The chaperone/usher secretion system represents the prominent machinery devoted to the production of these organelles [2–5]. This pathway uses a periplasmic chaperone that interacts with monomer subunits, protecting them from aggregation and proteolysis by forming chaperone-subunit complexes in the periplasm. So far, a variety of different gene clusters encoding for the proteins of this complex machinery have been identified [6]. Among these, the cluster deputed to the generation of P pili extensions in the uropathogenic *E. coli* is one of the best characterized [6,7]. P pili are composed of six distinct structural proteins that interact to form a composite fiber, formed by a rigid rod (68 Å diameter) which terminates with a thin fibrillum (20 Å diameter). The pilus rod is exclusively formed of PapA subunits arranged in a right-handed helical cylinder whereas the thin fibrillum is made mostly of repeating PapE subunits. PapA rod is anchored in the outer membrane by the PapH protein and to the PapE fibrillae by the PapK adapter protein. The P pilus terminates with the PapG adhesin, which is joined to the distal end of the tip fibrillum by the PapF adapter protein.

Structural investigations have provided enlightening information on the mechanisms of adhesive formation through the chaperone/usher secretion system [3,5,8–18]. These studies, initially focused on the chaperone and components of the fibrillae, have shown that all pilus subunits exhibit a noncanonical imunoglobulin-like (Ig-like) fold, since they lack the seventh *C*-terminal G strand and present, therefore, a large hydrophobic groove along the subunit. Except for the subunit PapG, all others possess an *N*-terminal region which does not interact with the rest of the protein. The association of the subunits is based on the binding of the *N*-terminus of one subunit to the groove of the adjacent one via a donor-strand complementation mechanism. The chaperone PapD assists the folding of all subunits and is important for their correct assembly in the final pilus. During the assembly of pili, which occurs at the outer membrane usher, the *N*-terminal region of an incoming subunit displaces the chaperone and occupies the groove of the last incorporated subunit (donor-strand exchange). A plethora of crystallographic studies have provided a solid base for the understanding of these processes at molecular level. However, some important aspects, mainly related to the structure and the role of transient species, are yet to be clarified. Various investigations have shown that molecular dynamics (MD) simulations are valuable in providing atomic level details of these complex processes, whose inhibition strongly depotentiate these

* *Correspondence to: Rita Berisio, Istituto di Biostrutture e Bioimmagini, CNR, Università degli Studi di Napoli "Federico II", via Mezzocannone 16, I-80134, Napoli, Italy. E-mail: rita.berisio@unina.it*

a *Istituto di Biostrutture e Bioimmagini, CNR, Università degli Studi di Napoli "Federico II", via Mezzocannone 16, I-80134, Napoli, Italy*

b *Dipartimento delle Scienze Biologiche, Sezione di Biostrutture, Università degli Studi di Napoli "Federico II", via Mezzocannone 16, I-80134, Napoli, Italy*

‡ *11th Naples Workshop on Bioactive Peptides.*

pathogens [14,19–21]. The very recent structure determination of the pilus rod subunit PapA in complex with the chaperone PapD offers the opportunity to analyze structural features of transient conformational states of this fundamental component of P pili [17]. Here we report extensive MD simulations on this subunit in its unbound state or bound to different fragments of the chaperone G1 strand. These analyses provide new data on the chaperone-subunit interactions and on the donor-strand exchange mechanism.

Materials and Methods

Starting Models

The starting coordinates of PapA subunit were derived from the complex between the chaperone PapD and two PapA subunits (PapD(PapA)$_2$) [Protein Data Bank (PDB) code 2uy6] [17]. Incomplete loops have been modeled using the program 'O' [22], followed by energy minimization with the GROMACS software package 3.3 [23]. Throughout the paper, recognition sites between the pilus subunit and the chaperone or the pilin *N*-terminal strand have been designated by adopting the notation used in previous studies (P1 to P5) (Figure S1) [17]. Various simulations were carried out both on the unliganded PapA subunit, on PapA bound to the G1 chaperone PapD strand (residues 100–112) (PapA–PapD$_{G1}$), and on two complexes between PapA and truncated forms of the PapD G1 strand (residues 102–112, PapA–PapD$_{G1\Delta P4}$, and residues 104–112, PapA–PapD$_{G1\Delta P3P4}$). In these latter complexes the G1 strand was deprived of residues occupying either the P4 or both P3 and P4 sites.

Simulation Procedure

MD simulations were performed using GROMACS 3.3 [23]. In all MD simulations, the model was immersed in a rectangular box filled with water molecules (Table 1). The GROMOS9643a1 (GROMOS96) [24] force field was used with the SPCE water model. The simulations were run with periodic boundary conditions. Systems were simulated in NPT ensemble by keeping constant temperature

Table 1. Parameters of the MD simulations

	Force field	Simulation time (ps)	Box (nm^3)	Water model	Number of water molecules
PapA–PapD$_{G1}$	GROMOS96	30 000	6.011, 5.146, 6.766	SPCE	6187
Unliganded PapA	GROMOS96	20 000	4.836, 6.198, 7.442	SPCE	6675
Unliganded PapA	OPLS	30 000	4.846, 6.319, 7.429	TIP4P	6772
PapA–PapD$_{G1\Delta P4}$	GROMOS96	10 000	6.011, 5.156, 6.766	SPCE	6206
PapA–PapD$_{G1\Delta P3P4}$	GROMOS96	10 000	6.011, 5.156, 6.766	SPCE	6216
PapA–PapD$_{G1\Delta P3P4}$	OPLS	10 000	6.091, 5.193, 6.828	TIP4P	6339

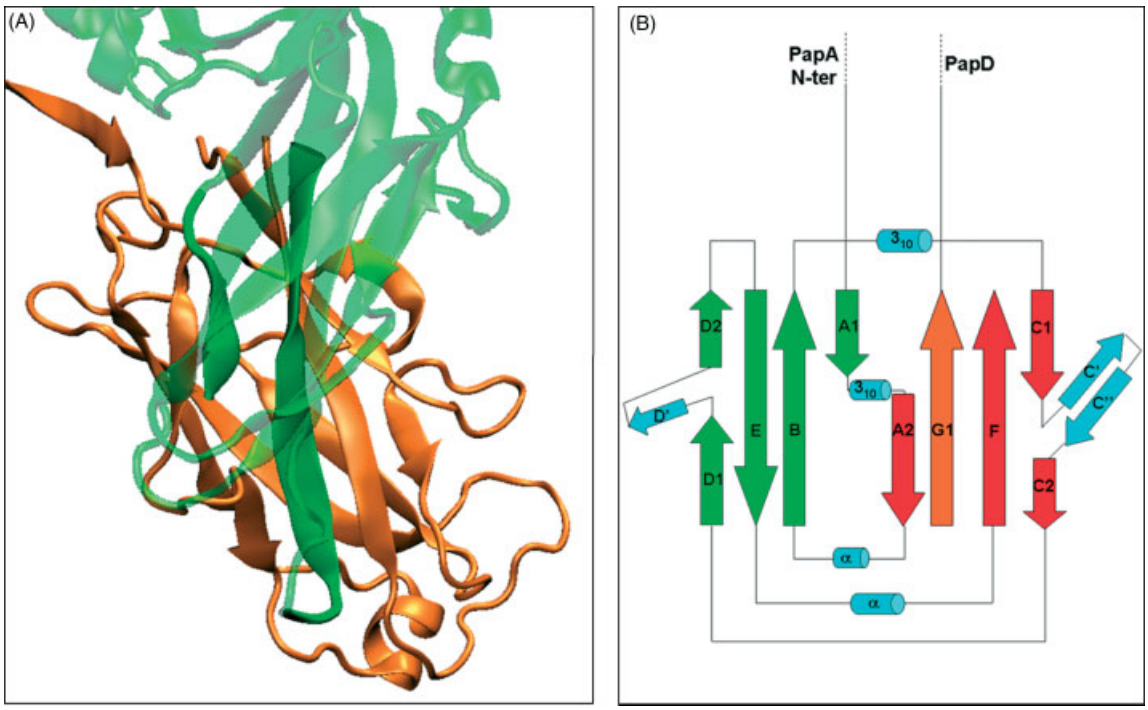

Figure 1. (A) Crystallographic model of the complex between PapA (orange) and the chaperone PapD (green). Regions of PapD, which interact with PapA in this structure are indicated in solid green whereas the rest of the chaperone is drawn in transparent material. (B) Topology of the PapA subunit in complex with PapD G1 strand (orange). The two facing β-sheets of PapA are drawn in green and red. The G1 strand of PapD (orange) complements the β-sheet containing A2, F and C strands (red).

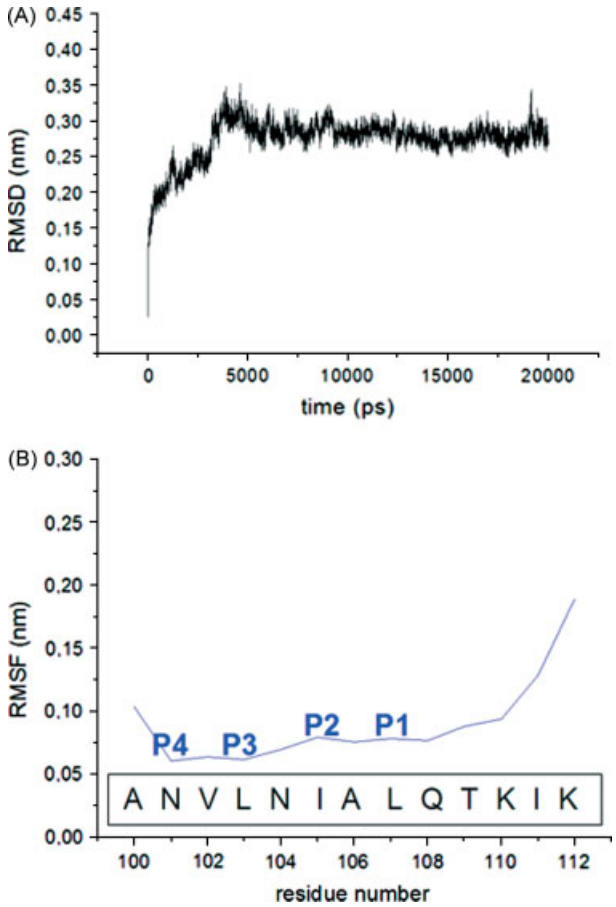

Figure 2. MD simulation of the complex between PapA and the PapD G1 strand, PapA–$PapD_{G1}$. (A) Evolution of RMSD values through the MD simulation of the complex PapA–$PapD_{G1}$. (B) RMSF values, calculated on backbone Cα atoms of residues belonging to the G1 strand in the equilibrated region (8000–20 000 ps) of the MD simulation. The sequence of the G1 strand is reported in the inset.

(300 K) and pressure (1 atm). To evaluate the dependence of results on the force field, MD simulations were repeated using the OPLS force field [25] coupled with the TIP4P water model (Table 1).

Before starting the MD simulation, 200-ps positional restrained runs were carried out for all the simulations. To check solvent relaxation effects, radial distribution functions of water molecules as well as protein–solvent interaction energies were analyzed. In the case of the unliganded PapA subunit, an MD simulation preceded by a positional restrained procedure (1600 ps) with a gradual release of protein degrees of freedom was also performed. This was achieved by running sequential positional restrained simulations with decreasing values of the force constant (fc). In particular, 1000 ps with $fc = 3000$, 200 ps with $fc = 1000$, 200 ps with $fc = 500$ and final 200 ps with $fc = 200$ kJ mol^{-1} nm^{-2}.

In all MD simulations, carried out with a time step of 0.002 ps and a dielectric constant of 1, bond lengths were constrained by the LINCS procedure. Lennard–Jones interactions were calculated with a 12 Å twin-range cutoff. Electrostatic interactions were treated using the particle mesh Ewald (PME) method with a cutoff of 10.0 Å. Trajectories were checked to assess the quality of the simulation using GROMACS routines and the program VMD [26]. We checked that in all simulations the lowest distance between the protein images was always larger than nonbonded and electrostatic cutoff values.

Results and Discussion

G1 Strand of PapD is Tightly Bound to the PapA Subunit

Initial MD simulations were conducted on the complex between PapA and the G1 strand (residues 100–112) of the chaperone PapD (PapA–$PapD_{G1}$). As shown in Figure 1, in the X-ray structure of PapA in complex with PapD [17], there are extensive interactions between the pilin and this chaperone strand. In particular, the A strand of PapA is composed of two portions, A1 and A2, separated by a 3–10 helix. A1 and A2 are located at one of the two edges of PapA groove. The β-sheet containing A2 is the one that is complemented by the PapD G1 strand (Figure 1). The evolution of the system during the simulations was monitored by using the indicators commonly adopted to check the system stability in MD analyses. The trend of root mean square deviations (RMSD) of the trajectory structures from the starting X-ray model shows that the (PapA–$PapD_{G1}$) reaches a stable state in the 8000–20 000 ps interval (Figure 2(A)). This observation is corroborated by the evaluation of other indicators such as secondary structure and gyration radius (data not shown). The analysis of the trajectory structures clearly indicates that the chaperone strand G1 is firmly bound to the PapA pilin. Indeed, H-bonding interactions between the strand G1 and the pilin persist throughout the simulation (Figure S2). As a consequence, the root mean square fluctuation (RMSF) values of strand G1 residues, computed in the equilibrated region of the trajectory, are rather low (Figure 2(B)). Notably, low RMSF values are also exhibited by the residues that are not bound to the P1–P4 recognition sites. This observation may be ascribed to hydrogen bonding interactions between residues of the G1 and F strands [e.g. between Thr109(O) and Leu160(N) and between Lys110(O) and Tyr162(N)], which are maintained throughout the simulation. Furthermore, although pilin–chaperone interactions in the crystal structure go beyond those established by the G1 strand, the removal of the rest of the chaperone does not affect the integrity and secondary structure elements of PapA (Figure 3). Altogether, these findings suggest that the extensive G1–PapA interactions are able to keep the system in a stable, well-defined state.

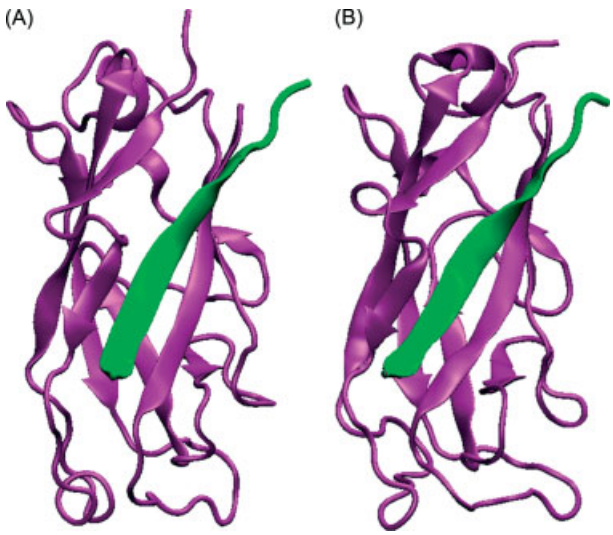

Figure 3. Ribbon representation of the starting model of the complex between PapA (prune) and PapD G1 strand (green) (A) and of a structure representative of the equilibrated region of the trajectory obtained with the GROMOS96 (B).

Dynamics of the Unliganded PapA Reveals a New Conformational State Accessible to the Subunit

The intrinsic conformational behavior of the Ig-like PapA domain (residues 20–163) in its unbound state was also investigated by MD simulations. These analyses were conducted by using, as a starting model, the X-ray structure of the sole PapA subunit, derived from the ternary complex PapD(PapA)$_2$ [17]. RMSD from the starting X-ray model indicate an early transition, which evolves toward a stable state after the first 7500 ps of the trajectory (Figure 4(A)). The plateau region of the RMSD plot is characterized by significant

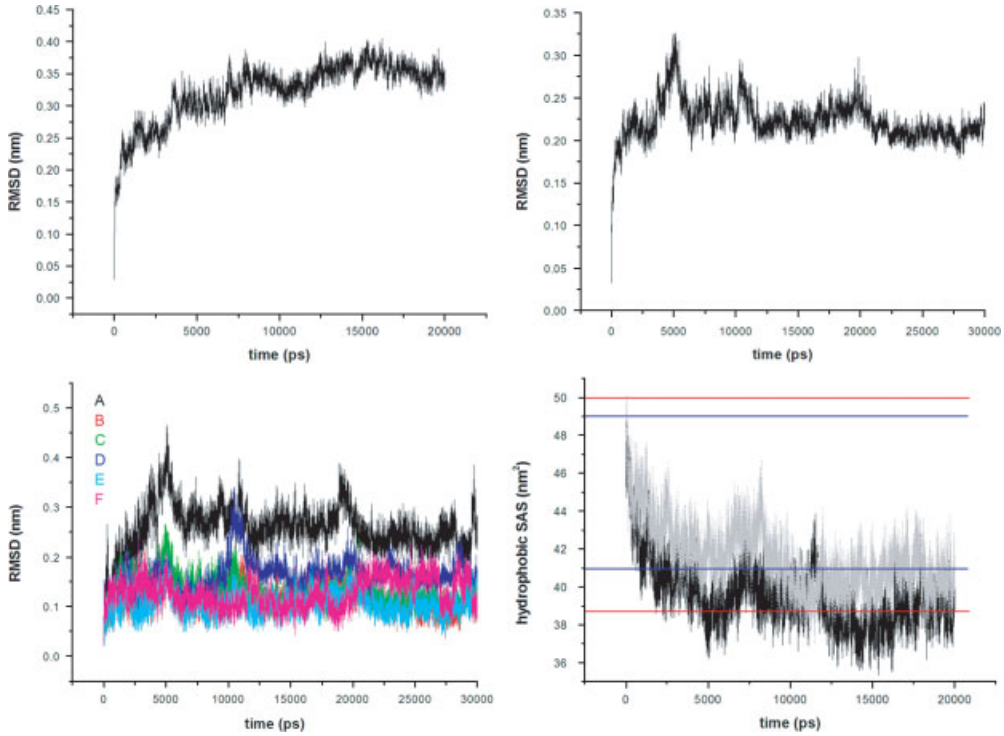

Figure 4. Evolution of RMSD values, calculated on Cα atoms, in MD simulations of unliganded PapA carried out with the GROMOS96 (A) and the OPLS (B) force fields. (C) Evolution of RMSD values, calculated on Cα atoms of A–F strands, throughout the MD simulation of unliganded PapA using the OPLS force field. Strands A–F are defined using PROCHECK. A: residues 23–25 and 32–35; B: 52–59; C: 77–82 and 89–94; D: 101–106 and 115–118; E: 130–139; F: 153–162. Color code is reported in the up-left inset. (D) Hydrophobic solvent accessible surface in the MD simulations of unliganded PapA (black) and PapA–PapD$_{G1}$ (gray). SAS values of the starting and equilibrated structures of PapA and PapA–PapD$_{G1}$ are shown as red and blue lines, respectively.

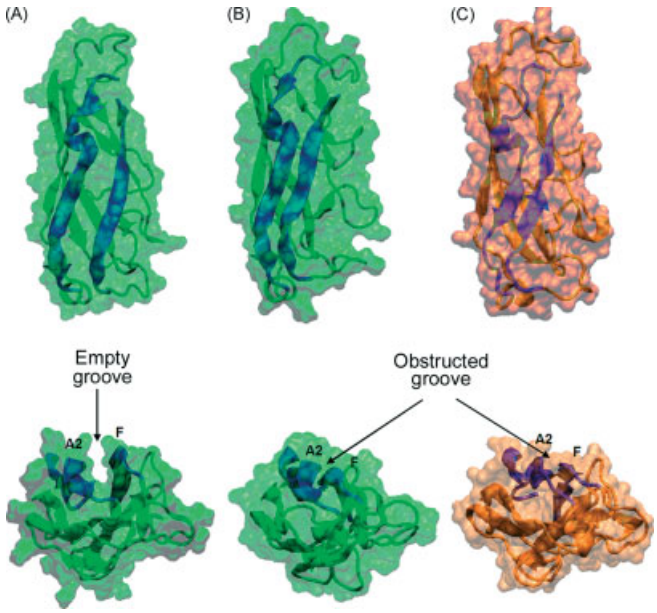

Figure 5. Ribbon representation and molecular surfaces of the starting X-ray model (A) and of structures representative of the equilibrated region of the trajectories obtained with the GROMOS96 (B) and the OPLS (C) force fields. The 90° views of (A), (B), and (C) are reported below. Residues lining the subunit groove are represented in blue.

deviations of the trajectory structures from the starting X-ray model (~3.5 Å). These deviations, which are higher than those observed in the simulation of PapA–$PapD_{G1}$ (~2.9 Å), are indicative of the structural modifications throughout the simulation. Analysis of the trajectory structures shows that the largest modifications affect the regions on the protein surface that were initially involved in the complex with PapD. Consistently, RMSD analysis of individual β-strands shows that the largest deviations are displayed by the A strand followed by the F and D strands (Figures 4(C) and 1(B)). This observation clearly indicates that PapA groove is unable to keep its open structure upon chaperone release. Both in the simulations of unliganded PapA and of PapA–$PapD_{G1}$, a clear decrease of hydrophobic solvent accessible surface (SAS) is observed. This indicates that the systems react by shielding surface hydrophobic regions generated by the release of the chaperone. In the case of unliganded PapA, which is also lacking the G1 strand, the reduction of SAS is more evident (Figure 4(D)).

A deeper analysis of the observed modifications shows that, once the PapD G1 strand is removed from the model, the A2 strand of PapA significantly moves form its position in the crystallographic PapD$(PapA)_2$ complex. Indeed, this strand, freed from the interactions with the G1 strand, comes closer to the F strand. In the equilibrated region of the trajectory, the interaction between A2 and F strands is stabilized by as many as nine backbone–backbone hydrogen bonds (Figures 5 and 6 and Figure S3). It is worth mentioning that, once formed, these interactions are maintained throughout the simulation. It is also noteworthy that, in contrast to A2, the strand A1 does not display significant rearrangements during the simulation (Figure S4) and remains associated with strand B. This leaves the extra region of the groove that extends beyond the P1 site in an open state. This finding is in line with the observation that in the PapA moiety of PapD$(PapA)_2$ complexed with the *N*-terminal peptide of the other PapA subunit this site is open, although it is not occupied by

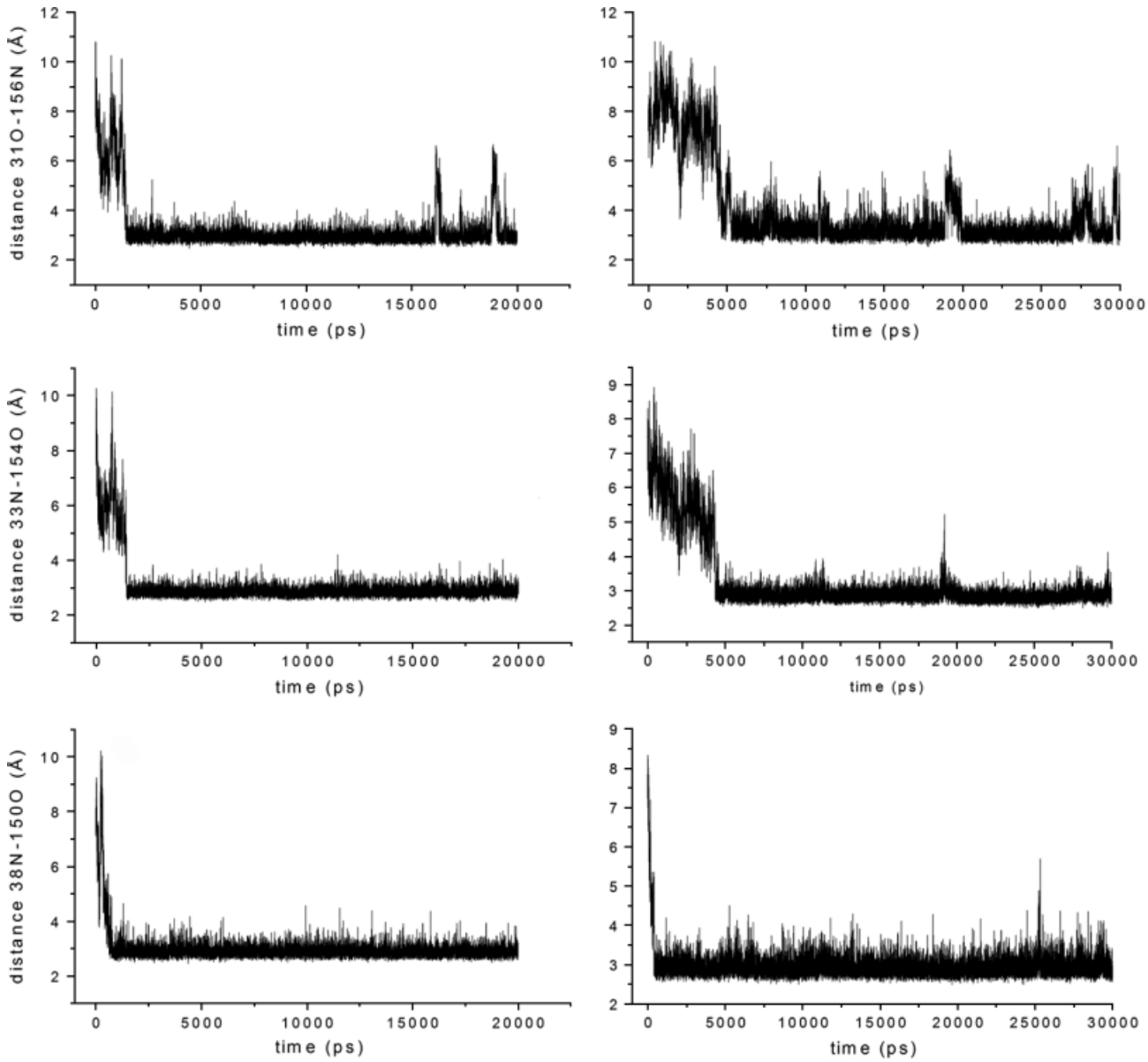

Figure 6. Evolution of distances between atoms forming H-bonding interactions throughout the MD simulations with both the GROMOS96 (left column) and the OPLS (right column) force fields.

Journal of PeptideScience

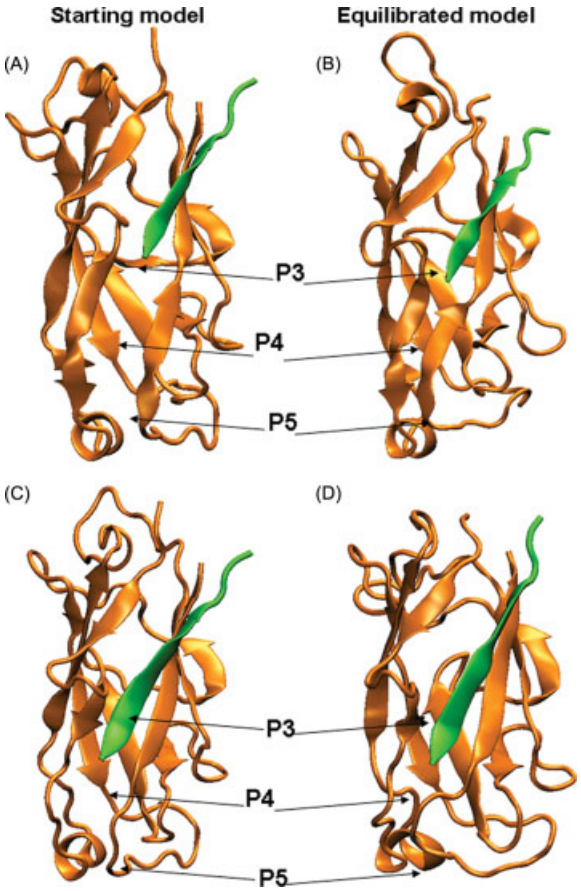

Figure 7. MD simulations of complexes of PapA with truncated forms of the PapD G1 strand. Ribbon representation of the starting models and of structures representative of equilibrated regions in the MD simulations of PapA–$PapD_{G1\Delta P3P4}$ (A), (B) and of PapA–$PapD_{G1\Delta P4}$ (C), (D).

any ligand [17]. Therefore, different regions of the groove display different behavior upon chaperone release.

The observed collapse of the PapA subunit was also confirmed by running another simulation, using the GROMOS96 force field, which was preceded by a longer positional restrained procedure (1600 ps) with a gradual release of protein degrees of freedom, see Section on Methods. The evolution of the system in this run closely resembles that observed in the previous simulation (data not shown). This indicates that the present findings can be reproduced even if different equilibration protocols are used. In addition, since it is known that the use of a specific force field may bias the results of MD simulations [27] we checked whether the large modifications observed in PapA simulation using the GROMOS96 force field [24] (see the Methods section for details) could be reproduced with a different force field. To this aim, this simulation was repeated by using the OPLS all-atom force field [25]. As shown in Figure 6, in this case, the equilibration process is slower. Nevertheless, a number of backbone–backbone hydrogen bonds between the strand A2 and the strand F are observed. Of the nine H-bonds formed in the simulation carried out by using the GROMOS96 force field, six are also observed in the simulation conducted with OPLS (Figure 6 and Figure S3). It is worth noting that the residues that form the three H-bonds observed only in the GROMOS96 simulation also come closer during the simulation carried out with OPLS. Therefore, although minor differences are observed in the two independent simulations, representative structures of the equilibrated regions of GROMOS96 and OPLS trajectories present similar features (Figure 5). Indeed, in both cases the groove region corresponding to the P1–P5 sites is completely obstructed due to interactions formed between the A2 and F strands. Along this line, the PapA extra groove region remains in an open state in both simulations, in agreement with the indication provided by the PapD$(PapA)_2$ crystal structure [17].

Role of the Individual Pilin/Chaperone Recognition Sites in the Donor Exchange Mechanism

The analysis of the simulations carried out on PapA in its unbound state clearly indicates that, upon chaperone release, this subunit has an intrinsic tendency to collapse. Since this novel state is not prone to polymerize through the donor-strand exchange mechanism donor, chaperone release and pilin–pilin association are likely concerted processes. The strikingly variable dynamic behavior of PapA depending on its binding state prompted us to analyze the dynamic properties of PapA bound to fragments of the G1 strand. This analysis on partially bound models was also aimed at providing information on potential transient states of the concerted mechanism that leads to the donor-strand exchange. In this framework, we carried out MD simulation of the pilin in complex with portions of the PapD G1 strand, which left either an empty P4 site (PapA–$PapD_{G1\Delta P4}$, including residues 102–112 from G1) or both P3 and P4 empty sites (PapA–$PapD_{G1\Delta P3P4}$, including residues 104–112 of G1). These simulations are intended to mimic PapA response to the gradual dissociation of the PapD G1 strand. MD simulations carried out on PapA–$PapD_{G1\Delta P3P4}$ clearly evidenced an immediate collapse of the PapA subunit (Figure 7). In this simulation, the lack of a residue blocking the P3 site allows for the association of the A2 and F strands through the formation of six backbone–backbone hydrogen bonds (Figure 8). These interactions compensate for the generation of unsatisfied hydrogen bond donors and acceptors upon dissociation of chaperone G1 strand from the P4 and P3 sites. Different results were obtained in the MD simulations carried out on PapA–$PapD_{G1\Delta P4}$. In this case, when the sole P4 site is left unoccupied, no major groove closure is observed (Figure 7). Indeed, the interactions formed in the simulation of PapA–$PapD_{G1\Delta P3P4}$, which would require a partial dissociation of the G1 strand at the P3 site, do not occur (Figure 8). Instead, only one rather transient hydrogen bond (between the carbonyl oxygen of Leu38 and the backbone nitrogen of Phe152) which does not form in the simulation of PapA–$PapD_{G1\Delta P3P4}$, is observed at the P4 site. These data indicate that the dissociation of the G1 strand of the chaperone PapD from the P4 site does not have a strong impact of the structure of the PapA subunit, which is still receptive for donor-strand exchange with an incoming PapA. Chaperone dissociation form the P4 site, without compromising the pilin ability to polymerize, may be important for providing enough space, required in a concerted donor-strand exchange process, for both an outcoming chaperone strand and an incoming pilin *N*-terminus.

Conclusions

The understanding pili formation, which is essential to bacterial pathogenicity, has received an enlightening contribution from biochemical and crystallographic investigations. There is increasing evidence, however, that computational approaches may fruitfully complement these studies by providing information on the

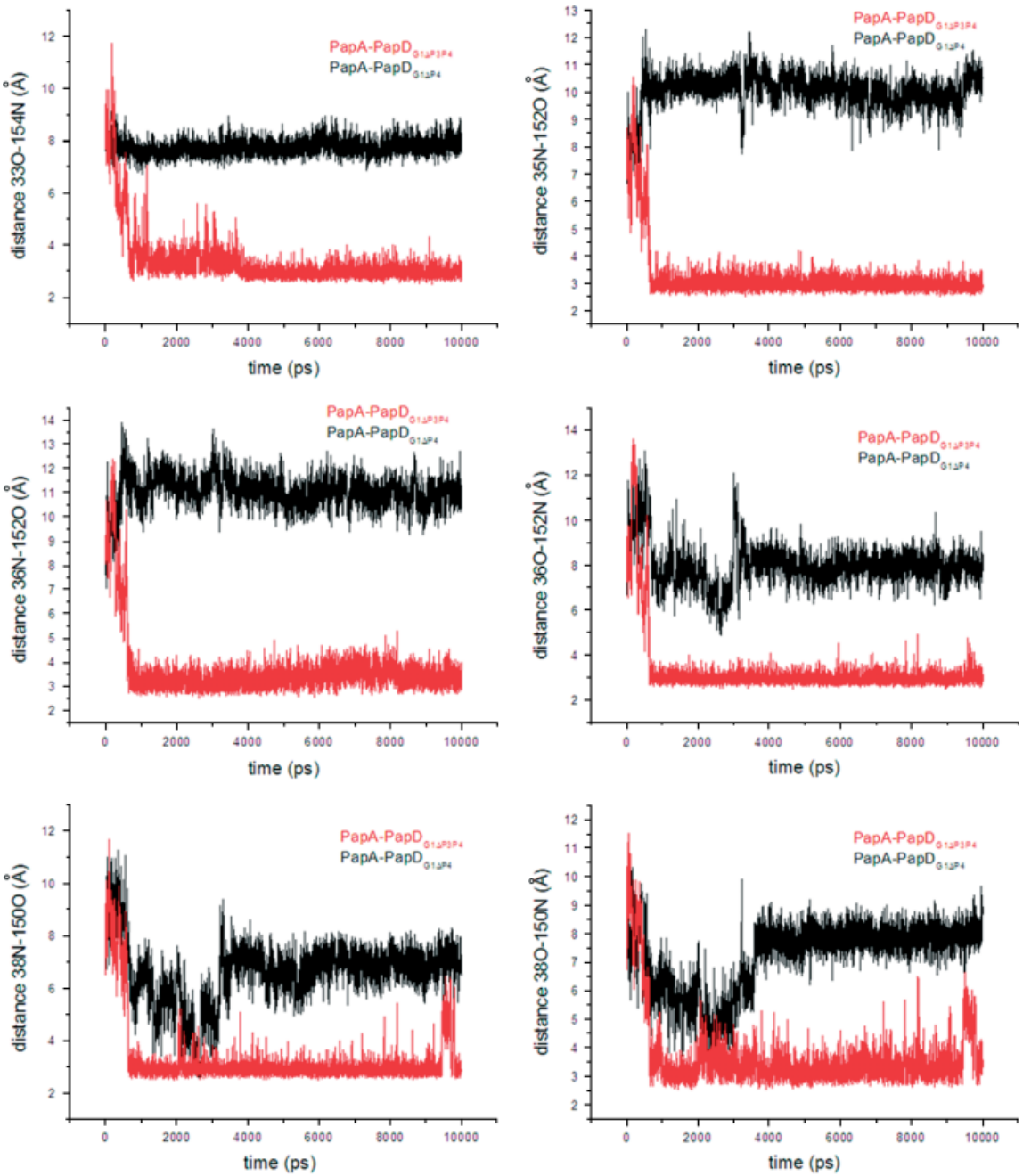

Figure 8. Evolution of the relative position of atoms belonging to the residues facing each other in the PapA groove throughout MD simulations of PapA–PapD$_{G1\Delta P3P4}$ (red) and PapA–PapD$_{G1\Delta P4}$ (black).

properties of specific conformational states whose experimental characterization is difficult. In previous investigations, we have shown that Ig-like domains of the uropathogenic *E. coli* PapE [19] and of Caf1 from *Yersinia pestis* [21] exhibit domain collapse when left in the unliganded form. A similar dynamic behavior has here been evidenced for the PapA subunit, the main constituent of P pili from the uropathogenic *E. coli*. Notably, this collapse of the structure likely hampers the subunit–subunit association process. Our new data along with the previous investigations [16,19,20,28] suggest that, in all systems involved in bacterial extension formation through donor-strand complementation, the chaperone has the important role to avoid quick collapse of the pilin structure toward states which are not prone to polymerize. This characteristic of chaperones is most likely the motivation for the concerted nature of donor-stand exchange mechanism. In this scenario, the strong intrinsic tendency of pilus subunits to undergo structural modifications in their unbound states is indicative of their high reactivity, which may be important for their tight association in the final fiber.

We also show that pilin domain collapse of the unliganded PapA occurs independent of the force field used and is, therefore, an intrinsic characteristic of the domain structure. It is well established that donor-strand exchange initiation occurs at the P5 site [29], which is empty in the PapA structure. We here observed that gradual release of the G1 strand of PapD from the PapA groove has increasingly strong structural consequences. When the sole P4

site is left unoccupied by the PapD G1 strand, no major changes occur at the PapA groove. This may leave an adjacent PapA subunit with the opportunity to insert its *N*-terminal part. More critical is the removal of the chaperone G1 strand from the P3 site, since an immediate groove collapse is observed.

In conclusion, our data provide further support to the concerted mechanism proposed for the donor complementation mechanism and also highlight the role played by the individual recognition sites present in the pilin groove.

Supporting information

Supporting information may be found in the online version of this article.

Acknowledgements

This work has been funded by the MIUR (FIRB-Contract number RBRN07BMCT). CINECA Supercomputing (project number 791) is acknowledged for computational support. We also thank Mr Luciano Ciccarelli for his help in data analysis.

References

1. Hooton TM, Stamm WE. Diagnosis and treatment of uncomplicated urinary tract infection. *Infect. Dis. Clin. North Am.* 1997; **11**: 551–581.
2. Sauer FG, Knight SD, Waksman Gj, Hultgren SJ. Papd-like chaperones and pilus biogenesis. *Semin. Cell Dev. Biol.* 2000; **11**: 27–34.
3. Sauer FG, Remaut H, Hultgren SJ, Waksman G. Fiber assembly by the chaperone-usher pathway. *Biochim. Biophys. Acta* 2004; **1694**: 259–267.
4. Zavialov AV, Kersley J, Korpela T, Zav'yalov VP, MacIntyre S, Knight SD. Donor strand complementation mechanism in the biogenesis of non-pilus systems. *Mol. Microbiol.* 2002; **45**: 983–995.
5. Zavialov A, Zav'yalova G, Korpela T, Zav'yalov V. Fgl chaperone-assembled fimbrial polyadhesins: Anti-immune armament of gram-negative bacterial pathogens. *FEMS Microbiol. Rev.* 2007; **31**: 478–514.
6. Soto GE, Hultgren SJ. Bacterial adhesins: Common themes and variations in architecture and assembly. *J. Bacteriol.* 1999; **181**: 1059–1071.
7. Dodson KW, Jacob-Dubuisson F, Striker RT, Hultgren SJ. Outer-membrane papc molecular usher discriminately recognizes periplasmic chaperone-pilus subunit complexes. *Proc. Natl. Acad. Sci. U.S.A.* 1993; **90**: 3670–3674.
8. Knight SD. Structure and assembly of yersinia pestis f1 antigen. *Adv. Exp. Med. Biol.* 2007; **603**: 74–87.
9. Sauer FG, Mulvey MA, Schilling JD, Martinez JJ, Hultgren SJ. Bacterial pili: Molecular mechanisms of pathogenesis. *Curr. Opin. Microbiol.* 2000; **3**: 65–72.
10. Holmgren A, Branden CI. Crystal structure of chaperone protein papd reveals an immunoglobulin fold. *Nature* 1989; **342**: 248–251.
11. Sauer FG, Pinkner JS, Waksman G, Hultgren SJ. Chaperone priming of pilus subunits facilitates a topological transition that drives fiber formation. *Cell* 2002; **111**: 543–551.
12. Sauer FG, Futterer K, Pinkner JS, Dodson KW, Hultgren SJ, Waksman G. Structural basis of chaperone function and pilus biogenesis. *Science* 1999; **285**: 1058–1061.
13. Zavialov AV, Berglund J, Pudney AF, Fooks LJ, Ibrahim TM, MacIntyre S, Knight SD. Structure and biogenesis of the capsular f1 antigen from yersinia pestis: Preserved folding energy drives fiber formation. *Cell* 2003; **113**: 587–596.
14. Zavialov AV, Tischenko VM, Fooks LJ, Brandsdal BO, Aqvist J, Zav'yalov VP, Macintyre S, Knight SD. Resolving the energy paradox of chaperone/usher-mediated fibre assembly. *Biochem. J.* 2005; **389**: 685–694.
15. Choudhury D, Thompson A, Stojanoff V, Langermann S, Pinkner J, Hultgren SJ, Knight SD. X-ray structure of the fimc-fimh chaperone-adhesin complex from uropathogenic escherichia coli. *Science* 1999; **285**: 1061–1066.
16. Remaut H, Rose RJ, Hannan TJ, Hultgren SJ, Radford SE, Ashcroft AE, Waksman G. Donor-strand exchange in chaperone-assisted pilus assembly proceeds through a concerted beta strand displacement mechanism. *Mol. Cells* 2006; **22**: 831–842.
17. Verger D, Bullitt E, Hultgren SJ, Waksman G. Crystal structure of the p pilus rod subunit papa. *PLoS Pathog.* 2007; **3**: e73.
18. Remaut H, Tang C, Henderson NS, Pinkner JS, Wang T, Hultgren SJ, Thanassi DG, Waksman G, Li H. Fiber formation across the bacterial outer membrane by the chaperone/usher pathway. *Cell* 2008; **133**: 640–652.
19. Vitagliano L, Ruggiero A, Pedone C, Berisio R. A molecular dynamics study of pilus subunits: Insights into pilus biogenesis. *J. Mol. Biol.* 2007; **367**: 935–941.
20. Rose RJ, Welsh TS, Waksman G, Ashcroft AE, Radford SE, Paci E. Donor-strand exchange in chaperone-assisted pilus assembly revealed in atomic detail by molecular dynamics. *J. Mol. Biol.* 2008; **375**: 908–919.
21. Vitagliano L, Ruggiero A, Pedone C, Berisio R. Conformational states and association mechanism of yersinia pestis caf1 subunits. *Biochem. Biophys. Res. Commun.* 2008; **372**: 804–810.
22. Jones TA. Interactive electron-density map interpretation: From inter to o. *Acta Crystallogr. D Biol. Crystallogr.* 2004; **60**: 2115–2125.
23. Van Der Spoel D, Lindahl E, Hess B, Groenhof G, Mark AE, Berendsen HJ. Gromacs: Fast, flexible, and free. *J. Comput. Chem.* 2005; **26**: 1701–1718.
24. Scott WRP, Huenenberger PH, Tironi IG, Mark AE, Billeter SR, Fennen J, Torda AE, Huber T, Krueger P, van Gunsteren WF. The gromos biomolecular simulation program package. *J. Phys. Chem. A* 1999; **103**: 3596–3607.
25. Jorgensen WL, Tirado-Rives T. The opls force field for proteins. Energy minimizations for crystals of cyclic peptides and crambin. *J. Am. Chem. Soc.* 1988; **110**: 1657–1666.
26. Humphrey W, Dalke A, Schulten K. Vmd: Visual molecular dynamics. *J. Mol. Graphics* 1996; **14**: 33–38, 27–38.
27. Mu Y, Kosov DS, Stock. G. Conformational dynamics of trialanine in water. 2. Comparison of amber, charmm, gromos, and opls force fields to nmr and infrared experiments. *J. Phys. Chem. B* 2003; **107**: 5064–5073.
28. Vetsch M, Erilov D, Moliere N, Nishiyama M, Ignatov O, Glockshuber R. Mechanism of fibre assembly through the chaperone-usher pathway. *EMBO Rep.* 2006; **7**: 734–738.
29. Verger D, Miller E, Remaut H, Waksman G, Hultgren S. Molecular mechanism of p pilus termination in uropathogenic escherichia coli. *EMBO Rep.* 2006; **7**: 1228–1232.

